J. Condensed Matter Nucl. Sci. 30 (2020) 1–24

Research Article

Nuclear Structure and Cold Fusion

John P. Wallace*
Casting Analysis Corp., 8379 Ursa Lane, Weyers Cave, Virginia 24486, USA

Michael J. Wallace
Phoenix, AZ 85050, USA

Abstract

Combining advances in understanding the strong force with experiments on lattice fusion allows a description of lattice D–D fusion to be constructed. What has to be exposed is a nuclear energy loss mechanism leaving little or no residual radioactivity. The requirements on the lattice for D–D fusion are strict and appear to be limited to particular FCC lattices within a range of lattice parameters. A mechanical understanding is needed of how elevated local concentrations of deuterium are achieved while avoiding being trapped at defect sites. Using optical, RF, and experimental anomalous heat data the metallurgical requirements for the process is refined by considering a combination of diffusion, partial molar volume, positron annihilation data, defect kinetics, and electronic band structure allowing logical exhaustion to identify the kinetic structure that drives lattice nuclear fusion.
 ISSN 2227-3123

Keywords: Cold fusion, Deuterium, Lattice, Metallurgy, Nuclear structure, Quantum mechanics

1. Introduction

In physics there are not many landmark experiments that use absolute measurements. Joule's conservation of mechanical and thermal energy, the Compton scattering experiment, the radiationless electron scattering ionization of the hydrogen 1S state [1], and now cold fusion experiments producing transmutations at thermal energies. Most experiments are done with differential measurements comparing two similar states where there has been a transition either atomic or nuclear. Such simple comparisons shields the experimenter from the responsibility of having an accurate description of the state's structure because of the differential nature of the measurement. Lattice cold fusion cannot be treated by such a simple approach.

Lattice cold fusion that is initiated by gas phase charging has the lowest input energy of all the non high energy methods that drive transmutation. This particular process represents the minimum in material and energy overhead required to drive a nuclear reaction. It is this very economic process that needs to be understood.

*E-mail: jpw@castinganalysis.com.

 ISSN 2227-3123

The advantage in studying cold lattice nuclear processes is that a window opens on a number of poorly understood areas: solid state interstitial behavior, nuclear structures [2], crustal transmutations [3], dust fusion [4], and the role of condensed plasmoids [5]. By beginning with the behavior of the hydrogen isotopes on the interstitial FCC lattice initiating a nuclear process at thermal energies sets the minimum conditions for the fusion process. The physics supported by these transmutation processes openly questions the validity of a number of models about nuclear structure, the earths crustal chemistry, standard solar model, along with the current dogma that claims the electron neutrino possess mass [6,7]. The reward in making a mistake on such a basic physical process as fusion is to have all that was built without its use brought into question.

The prime difficulty in understanding the conditions for D–D fusion in the solid state is that scale properties from lab dimensions down to nuclear scale all come into play. To explain the process a path has to be constructed through these descending scales. If a mechanism for D–D fusion can be defended then the slightly higher energy mechanisms that alter the heavier element distribution by both fission and fusion in the earth's crust and space can be more easily approached.

2. Crystal Structure and Lattice Parameter

Successful experiments supporting cold fusion that have had their details published appear to have a common thread: a favored crystal structure and a narrow range of lattice parameters supporting the process. Latticed parameter can be affected in three ways, damage induced strains, [8], alloying [9,10], high thermal gradients [11], and by a combination of these methods. By alloying, the lattice parameter can be adjusted in three ways, alloy to a single composition, have a concentration gradient by diffusion between two metals, i.e. Cu–Ni or mechanical alloying at an interface, example Ni–Pd. When alloyed to single composition a strong thermal gradient seems to be required for having active sites as heat is produced and the internal temperature gradient alters the lattice parameter locally.

Our focus will be on cold fusion experiments reported for palladium, nickel, their alloys, and nickel–copper alloys, Table 1. Titanium would be the odd metal in this group as it is crystal structure is HCP and not FCC. However, with a stacking fault generated in deformation, there are FCC transformed local regions in deformed titanium.

Popular theories for describing lattice enhanced fusion tend to stress increases in lattice volumes due to vacancies in super abundance [12] and other large defects such as microcracks [13]. Neither model supplies a compact confinement structure required for fusion, but rather supplies excess volume. This excess volume comes from vacancies created during the deuterium charging process where the metal is damaged as a precursor for microvoid formation, which is necessary step in collecting then discharging the light ions into a supersaturated lattice on microvoid collapse. From the initial experiments of Fleischmann and Pons the damage and metallurgical recovery process has been part of the cold fusion prescription. Recovery via microvoid formation and collapse has been studied by positron annihilation [14,15], however, it has never been fully explained in detail. The creation of vacancies, their collection into microvoids, hydrogen isotopes being captured in the microvoids, and the microvoid collapse are all essential features of the damage driven D–D lattice cold fusion process, but are only the preliminary steps to the final fusion. It was shown studying hydrogen behavior in iron that only when hydrogen has been purged from the material, does the positron long life time component vanish, which had been long associated with the presence of microvoids [16]. A clean internal microvoid not coated with hydrogen or deuterium presents no barrier for the conversion of a trapped triplet positronium, the long lived species, $\sim$1000 ps, to singlet positron that promptly decays with a short lifetime, $\sim$100 ps. The measured long life times in damaged metals appear not to be a signature of the presence of microvoids, but microvoids with internal surface contamination that can preserve the triplet state of positronium. The principal contaminants found in microvoids are the fast diffusing hydrogen isotopes.

Recently it appears that the requirement to do damage prior to charging in monolithic metal host may have been overcome by Mizuno in a process of mechanical alloying where he transferred palladium to a fine nickel screen by

Table 1. Even though the coefficient of thermal lattice expansion differs by ∼10% between palladium and nickel based on their lattice parameters the difference is only only 0.3% which in part explains the complete solid solution over their entire range of temperature and composition. This coupled with their matched mechanical elastic modulus sets up the condition that grain boundaries might not be highly favored interface structure at a nickel–palladium interface allowing the boundary to reconstruct with the composition change occurring over a few unit cells. The other unique feature for the pair of metals is the peak in electron density at the Fermi surface compared to other metals allowing enhanced ion screening [31].

Element	Lattice Parameter	$\frac{m}{m^\circ \mathrm{K}}$	Bulk Mod. GPas.	e^- state density
Cu	3.597	16.7	123	.3
Ni	3.5168	13.0	180	4.8
Pd	3.8827	11.8	180	3.2

rubbing [10]. This process of mechanical alloying solved two long standing problems. One to provide easy entry of hydrogen to a reaction zone via the palladium free surface, while creating an array of interstitial sites with varying volumes from what is found in undamaged nickel to that of undamaged palladium. These will be distributed through the interface of the two metals and constitute the result of mechanical alloying. It is not only a particular interstitial volume that will be important as an active site it is also having other sites with slightly different volumes active as temperature changes. This range of sites must exist in quantity.

2.1. Unique metallurgical site

There are a number of lattice assisted cold fusion experiments reported for palladium, nickel, their alloys, nickel-copper alloys and titanium. The hydrides and deformed regions of these metals, which are generated on hydrogen isotope charging, are of less interest in the final act of driving a fusion process because they represent regions of increased volume that can trap and isolate the hydrogen isotopes as atomic species with a bound electron. This is evident in the atomic transitions of the triplet to singlet atomic deuterium transition at 327 MHz in the recent experiments by Swartz [17]. What is required to drive fusion is a strong, compact, symmetric, and constrained cavity. The deformation pathway to cold fusion needs three precursors: first to generate vacancies that form microvoids for collecting hydrogen isotopes that can then be discharged on collapse. Second is to introduce damaged regions in the crystal as a whole, putting the undamaged FCC regions in a state of increased tension for nickel and compression for palladium, and third to increase the anharmonic potentials between the undamaged FCC regions and the damaged volumes.

The metals have to be viewed as a mixture of undamaged and damaged portions some of which maybe hydrides. This overall damage is driven by the large partial molar volumes of the hydrogen isotopes [18] facilitating the occupancy of the interstitial octahedral sites with a pair of deuterium ions. Two deuterium occupying a single site is favored over two protons because of the smaller dynamic volume of the deuterium ion on the tightly constrained interstitial site due to deuterium's greater mass.

The FCC structure is of interest because of its high symmetry both on the atom site, but also on the highly

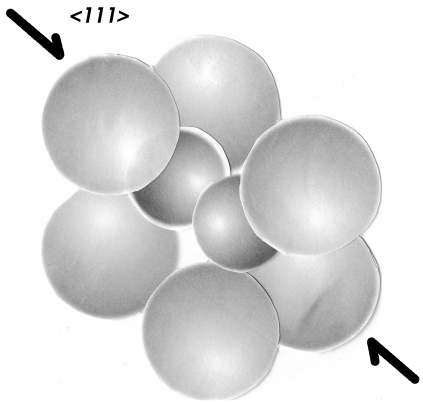

Figure 1. Two deuterium ions oriented along a $\langle 111 \rangle$ axis in the FCC octahedral interstitial site. Even though this same geometry of eight elements can be reproduced in the HCP lattice the cubic symmetry of the restraint provided by the rest of the lattice is lost along the three remaining equivalent orientations of the FCC site.

symmetric regular octahedral interstitial site. This combination is unique and not found in any other metal crystal systems. All other interstitial sites are irregular and of lower symmetry. The FCC octahedral site is a large site compared to other FCC and BCC interstitial sites and with six metal atoms coordination forms a cage capable of packing two interstitial D ions and holding them together in close proximity, Fig. 1. The FCC lattice unlike the diamond cubic lattice is a densely packed cubic structure. The utility of the FCC lattice's octahedral site for cold fusion is that it can act as a closed die forge where there are 4 independent $\langle 111 \rangle$ axis available for constraining two D ions making their capture much easier and escape more difficult. Each deuterium ion is cradled by three metal atoms minimizing the D ion from slipping laterally. If it does slip it will be captured by another three metal atom barrier of the site. This is where the four independent $\langle 111 \rangle$ axis along which D–D contact is constrained, eliminates an easy escape from the closed die forge the site creates. Just as important is the symmetric coordination of the supporting metal atom, that is 12 in the FCC, and this symmetry is lost in the HCP and BCC lattice. The coordination of six for the octahedral FCC interstitial site is high for an interstitial site, but the necessary minimum to support two trapped ions per site. The BCC octahedral site is not symmetric and squashed along the cube axis. Neither micro-cracks nor super abundant vacancies provide the constraints to bring two D ions in close proximity as does the FCC octahedral interstitial site to drive fusion.

The atom site or vacancy site on the FCC lattice has 12 nearest neighbor coordination, however, the central site sees six cube faces on the three principal cube axis. The cube face does not provide the same constraint for compression as the interstitial faces which are composed of three nearest neighbors.

Two different experiments were key in drawing our attention to the high symmetry sites in the lattice as being critical to drive nuclear activity. These experiments were the Raman measurements of Stokes/anti-Stokes lines [19,20] and the dual laser beating [13], that in both cases are sampling the energetic optical phonon. There are two high symmetry points in the FCC lattice: the atom site and the median edge site that is also the location of the interstitial octahedral site.

2.2. Anharmonic compression

Fusion is inhibited by electrostatic repulsion of ions and can be reduced by dynamic screening, however, an additional mechanism is required to drive the ions together. In the deuterium charged lattice there are regions of hydride formation and significant damage and regions of undamaged FCC lattice with interstitial deuterium. This composite material will lose its normal low amplitude linear elastic properties as the anharmonic terms can grow with the increased concentration of deuterium on the interstitial lattice. It has also been pointed out that fusion will be assisted in anharmonic regions by the periodic localization of high intensity lattice vibrations first studied by Fermi, Pasta and Ulam and recently being considered as a way to enhance catalysis, both chemical and nuclear [21]. For this mating process to drive fusion a compact lattice structure is needed to push the two ions together along with a dynamic screening process to suppress the repulsion.

2.3. Interstitial sites metallurgy

One of the most powerful tools in understanding interstitial behavior in metals are the activation energies for diffusion. If they are large then the diffusion process can be treated in the tradition classical way of using a configuration energy barrier which must be overcome. However, the activation energies fall into the range ~ 0.1 eV or less then the classical model fails. For the light interstitial such as the hydrogen isotopes imaging them is not possible. One nice feature of the activation energy of diffusion measurements is that the fast diffusion processes are not masked as the slower process can be masked. The most extensively studied couple is H–Fe where hydrogen is a very rapidly diffusing species with an activation energy of 0.047 eV, where there are a number of failure mechanisms in which hydrogen participates. There is a large mass effect for deuterium whose activation energy is 0.082 eV in iron. These small activation energies are dictated by two characteristics, first the light isotopes are in a very compact site and cannot be screened, they are naked ions. They behave as bare charges and strongly perturb their sites expanding them that is revealed in their significant measured partial molar volumes. The second feature affecting the activation energy is the potential well depth, which can be computed from a quantum model that is consistent with the activation energies of the three hydrogen isotopes [22].

The metallurgy of the hydrogen isotopes in the FCC metals is more complex because of the large site size for a single interstitial occupant. The advantage for fusion in the FCC metal are the interstitial potential wells are not that shallow allowing a high energy non-equilibrium configuration of interstitial pairs. Nickel and palladium share three characteristic that are important relative to the behavior of the interstitial isotopes of hydrogen. The hydrogen interstitial sites for nickel and palladium are rather deep and have nearly the same activation energy for diffusion. Indicating their sites are rather similar even though their lattice parameters differ. The highly symmetric location for the principal octahedral interstitial site and the high symmetry of the site itself in FCC metals makes it a more flexible site to abuse without destruction by the addition of a second interstitial. There is no preferred orientation for a distortion as would be the case for a lower symmetry site. In the BCC lattice the interstitial sites do not have a high symmetry that leads to axial distortions and instability with a single interstitial and collectively leads to problems of embrittlement, blistering, and attack found in iron and niobium [23].

The macroscopic laboratory scale comes into play when trying to determine where in a metal lattice such process should occur. One can force the lattice parameter of a material to lower values through hydro-static compression, however, the same is not easily accomplished in expanding the lattice. It is easier to expand the lattice nearer to a free surface and this is where damage caused by hydrogen or deuterium charging is predominately found, within a micron of the surface and where cold fusion was traced by transmutation products [24].

Table 2. Metallurgical preliminaries required for damage controlled cold fusion.

Substrate
Solid state process not liquid state at 1 atm.
FCC not BCC
Ni & Pd band structure
^{2}H Mass favorable for interstitial binding
Loading → Slow
High gradient strain fields from ^{2}H loading
Dislocation formation and flow
Vacancy generation
New phases
Microvoid formation
Recovery → More rapid
Near surface strain relaxation gradients
Vacancy trapping of ^{2}H
Vacancy diffusion to free surfaces
Microvoid enrichment with ^{2}H
Microvoid collapse → Fast
Charge stripping of ^{2}H from collapse
Inject the lattice with high interstitial conc.
Double site occupancy
Local current for dynamic screening
D–D fusion

2.4. Damage mediated cold fusion and dynamic recovery

Electro-chemical, plasma, or vapor phase charging of either nickel or palladium with deuterium drives the alloying of the metal with hydrogen isotopes. It is difficult to describe this process as a simple steady state process because the state of stress in the disturbed volume varies continuously going into the material leaving a wake of damage that affects both the diffusion front and the stress state within the metal. This process does not move as a simple plane front, but produces both islands of damaged material in an undamaged matrix, analogous to a two phase mixture. The ability of strained sites to expand changes as both a function of depth and damage. The problem is damage is continually induced into the metal, which will try to recover via different pathways [25]. The near surface has a major effect on the damage profile and the local strains achieved in the lattice, Table 2.

The question that is necessary to ask is how can a lattice be primed with a high concentration of non-trapped interstitial deuterium that will produce a small population of di-deuterium interstitial? Two dynamic processes are required. One is to remove the population of free trapping sites for deuterium while also dumping a quantity of free unscreened interstitial deuterium onto the interstitial lattice. This is essential in order to get sufficient concentration so that two deuterium can for a short time share the same interstitial location.

Nano-structures are helpful because of the large surface area with a reduced strain energy for expanding an interstitial site near a free surface. The process of recovery is one where vacancies generated by the strain induce charging damage diffuse and collect into microvoids. These microvoids will eventually collapse and generate prismatic dislocation loops as a signature of their former existence. Positron annihilation lifetime measurement of the long lifetime component and its intensity can also be used to study microvoids, because the long lifetime component is found in deformed metals with both FCC and BCC structures [15]. However, the interpretation of the data requires some care.

A common way is to take a the long lifetime component as a measure of multiple vacancies in a clusters. The argument of Sakai that the long lifetime component is proportional to size of the vacancy cluster is flawed, because within a microvoid with more than a few vacancies positronium can form in either of two states: triplet or singlet. The singlet state has a very rapid decay on the order of 100 ps The triplet state more than 1000 ps. In a microvoid where the interior surfaces are clean, meaning not covered by a monolayer of adsorbed interstitial, then the conversion of triplet to singlet state should be quite rapid and there should be no long lifetime component. This was confirmed in deformed iron that had been purged of hydrogen [16], where the long lifetime component vanished.

Purging hydrogen from metals is not a simple process requiring vacuum melting and long high temperature anneals in a hydrogen free atmosphere with external hydrogen getters. Normally in deformed metals containing trace hydrogen there is a strong long lifetime component in deformed and recovered specimens. Dynamic recovery when microvoids are generated sees their population drop on recovery. If these microvoid interior surfaces are covered with hydrogen, then this hydrogen will be dumped into the latticed on the microvoid's collapse creating a local super saturation on the interstitial lattice. A local super saturation of deuterium will supply ions to doubly occupy the FCC octahedral sites and precipitate a nuclear fusion. Unfortunately, the penetration depth of positrons is on the order of 10s of microns, greater than the 1 micron depth found for transmutations, which limits its utility as a near surface probe for damage [24].

3. Dynamic Screening

Complicating atomic, solid state, and nuclear physics is the failure in standard quantum mechanics to develop structural information about electron and nuclear structures, which has inconveniently left the analysis of cold fusion in limbo. Quantum mechanics is an incomplete subject poorly treated by mathematicians who forced the subject into forms they are familiar with. Because of a failure to strictly conserve total energy during its development from 1927 to 1934, relativity was not properly treated. The first of these mistakes was taking the form of the Dirac equation as being good relativistic description for the electron. This is evident because it fails to generate a physical ground state for the 1S hydrogen atom [26] principally because it is a linear approximation of a second order equation. Dirac in 1932 tried to back away from this method but failed to find an alternative method [27]. This left a legacy that relativity in quantum mechanics could be treated with a first order equation. Following WWII there was a race to find the corrections to non-relativistic Schrödinger equation solution for atomic hydrogen, which also was an approximation. The experimental advances made by Kusch [28] and Lamb [29] was in part to provide information not only about atomic properties but also nuclear properties. The nuclear contributions were completely ignored by the race to produce quantum electrodynamics. Small corrections to a damaged theory of non-relativistic quantum mechanics does not ensure a correct theory particularly if non-unique methods were employed. Starting with these mistakes, high and low energy quantum theories diverged to increase the confusion over the years. What was lost was a structural description of fields and matter. This can now be treated with differential equations that describe quantum structure derived directly from the relativistic energy conservation relations [30,2].

To understand dynamic screening by the lattice electron of two closely confined positive ions requires knowledge of the electron's charge structure. The electron structure comes directly from its field structure and its charge density is plotted in Fig. 2 [1]. The scale of the electron's charge density determines the scale of minimum approach of two ions without supplying additional energy, when screened by the dynamics of the lattice electrons. Attempts have been made to explain dynamic screening by a compact electronic structure by using fractional quantum states from the Schrödinger equation and deep lying states via the Dirac equation. These approaches fail in two ways: the deep states have never been detected in scattering experiments and the approaches fail to produce structural information about the electron.

Palladium and nickel are unique among the metals in the structure of their available valence electron density of

state just at the fermi surface, showing a very large density of available electrons that can be activated with a minimum of energy to provide dynamic screening currents between the positive ions, Table 1 [31]. This near singularity in density of states enhancement approaching the fermi surface is not found in any other FCC or BCC metals.

Screening as computed from density function theory is handled as a static polarization of the valence electrons including the exchange and correlation effects that works well at low density metals or at low density molecular orbital. However, in the compact region of the interstitial sites that deuterium occupies, the small scale structures cannot be screened by this quasi-static mechanism where density function theory fails at its lower bound [22]. An alternate mechanism for screening the two ions is required. A process to dynamically screen a free charge is available in nickel and palladium, because of the unique band structure in nickel, palladium, and their alloys with a high density of states at the fermi surface permits currents to be generated from the minimal electrostatic attraction of the deuterium ions. This characteristic band structure is also the source of the catalytic abilities found for these two metals. The location of the octahedral site on a cube edge allows 6 separate currents to be generated while maintaining overall charge neutrality. The cubic symmetry of the site allows for this multiplicity of current to dynamically screen two deuterium ions and drawing them together in any of their four possible orientations on the octahedral site, Fig. 3.

The limits to this screening is controlled by the structural dimension of the electron charge distribution. The electron has a structural charge radius on the order of $\hbar/mc \sim 4 \times 10^{-13}$ m which now becomes the minimum scale where complete screening can occur [1]. The process of dynamics screening can take on a second role when the ions are close and energy is being shed to the electrons as nuclear binding progresses. This second role is the removal of energy via a potential interaction with the altered nucleon charge density distribution. Such direct interactions have been postulated to provide a means of incrementally removing the mass defect energy from the nucleus and dumping it into the lattice via electron scattering to an increased phonon population [32]. Recent accelerator experimental data have found a positive result in the study of H–D fusion in a solid target where the energy removed in less than 10% of the reactions was by an electron [33]. This was not weak decay process but a prompt lattice electron that was ejected with the excess characteristic fusion energy.

4. Nuclear Structure

Having found a way to get two nuclei in close proximity it is now necessary to understand how the strong force functions to produce a fusion reaction. Fusion even in the core of the sun at its elevated pressure and temperature is not a common phenomenon. It is only the sheer volume of the sun that allows it to produce sufficient heat to bring its surface temperature to $\sim$5700°C. To study cold fusion knowledge of the strong force is essential. There are few scattering experiments that produce unambiguous information about the strong force. One of these experiments will be used to test a model of the strong force so it can be used with confidence in describing fusion. In accelerator experiment to drive D–D fusion there is no lower bound cut off found experimentally for this process down to the 10 keV range and that might indicate that at low energies polarization of the approaching nucleons are affected not only by electrostatic polarization to reduce the interaction barrier but also strong force polarization of the deuterium.

To excise the concept of a point charge in nuclear structure requires a look at the late 19th century attempt by mathematicians to perfect analysis, the calculus. The idea that the mathematical continuum does not represent a physical space where quantum mechanics can be produced was never seriously considered during the 1930s. The quickest way to understand the importance of this omission is based on a two part argument taken from the work of Georg Cantor the 19th century mathematician concerned with the orders of infinity [34]. Cantor proved a series of theorems about the mathematical continuum and one of these theorems stated that with a continuum defined space, dimensions become only a labeling scheme [35]. Dimensions are not a unique or necessary features of the continuum's mathematical landscape other than as a flexible accounting mechanism. The indexes defining the dimensions can be rearranged at will and are not uniquely associated with a particular dimensional structure of space. Physically, there is

considerable experimental evidence that spatial dimensions are real, definable, and a necessary delineation for defining a physical space. Particularly, for defining the properties of the one and two dimensional components of the baryons, the quarks. Dimensions are the major component in defining a quantized charge and the structure of matter and are not an arbitrary convenience. The inescapable logical deduction is that a physical space cannot be represented by the continuum, and must be replaced with a less compact description where dimensions have physical meaning.

To be consistent with relativity and the conservation of energy, two spaces are required, one to define the self-energy of an individual particle or a field, named the self-reference frame, and the second space is the normal laboratory frame for dynamics where measurements are made. These spaces are statistically independent, bring in the probabilities of quantum mechanics. With this change, the point mass and point charge of classical physics are lost [2,30].

The observer [36,37] is not an essential part of the measurement for the particles and fields because they are individually subject to comparisons by their dual descriptions in both the self-reference frame and laboratory frame. The two complementing frames of reference are statistically independent, eliminates the need for an observer. The comparison captures the limitation on the scales that can be used in describing physical behavior and concurrently defines the limitation of their space. This same mechanism can then be used to describe higher level emergent processes. The structure of the electron is of importance in that its scale and charge distribution define the lower limit of where dynamic screening becomes ineffective.

In this new view of quantum mechanics potential generated forces have their origin in the structure of the particles themselves. For these potential generated forces there is no need to invent an exchange boson to carry the force. These potential generated forces are essentially contact interactions over a volume. This removed the difficulty in explaining the origin of the electrostatic interaction.

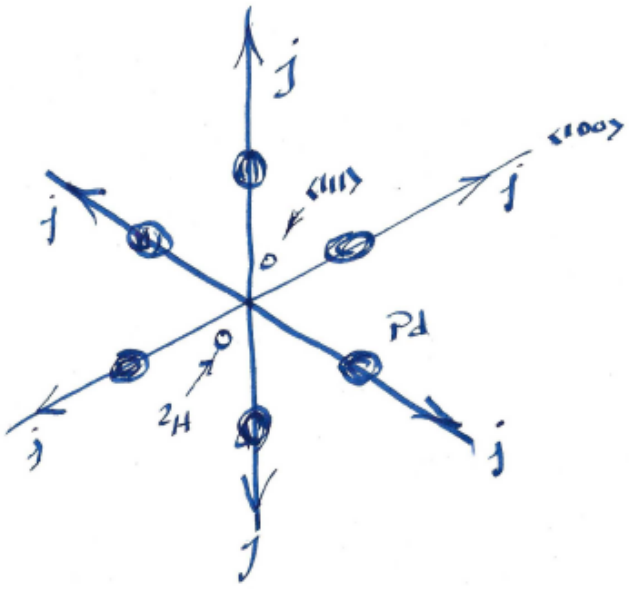

Figure 2. The electronic currents, *j*, along the cube axis dynamically screen the deuterium ion pair centered on the octahedral interstitial site.

4.1. Nucleons

Experiment has revealed the protons and neutrons are composite particles constructed of fractionally charged components. Nucleon structures were not revealed in those experiments. These components can be constructed from the lower dimensional massive solutions found in the self-reference frame [30]. These solutions in product combination generate the particle structure. Yet the components are not individually isolated from each other as was originally thought from the early electron-scattering parton experiments [38]. The early nuclear model was complex. A family of fields was postulated in the early 1960s called gluon to hold the components together by their exchange [39]. Though none have ever been detected, they were assumed to exist because of three jet decays found in high energy collisions. This was not a direct observation of the gluon and thus a very tenuous explanation. The gluon picture of nuclear structure will not be used. Recent high energy experiments now support a structural description of the baryons. Deuterium's ground state which is the simplest bound state of two baryons can be modeled by only considering the overlap in the two nuclei state functions. A second high energy form of deuterium can also be modeled, which occurs when the proton is driven into the neutron during a short range correlation by a high energy electron [40]. This state can be modeled by just using the product state of the six lower dimensional quark components [2].

Using the description of the two lower dimension fermion fields, 1D and 2D, as defined in the self-reference frame to represent the up and down quark. What is meant by lower dimensional components are not Euclidean lines and planes rather functions where volume is defined as $V \sim a^n$ where *a* is a scale and *n* is the dimension. These fields can be found as the spatial solutions from equation 1 which is derived from the relativistic conservation relation for the dimension $n = 1$ and 2, κ is proportional to mass and is one over the particle's scale ϵ, and γ is from relativity scaling the relative motion [2].

$$\frac{\partial^2 \mathbf{u}(r)}{\partial r^2} + \left(\frac{n-1}{r} + \kappa\{1 - i\gamma\} \right) \frac{\partial \mathbf{u}(r)}{\partial r} - i\kappa^2 \gamma \mathbf{u}(r) = 0. \tag{1}$$

This equation generates solutions for both fermions and bosons in the particles self-reference frame, where ${}_1F_1$ and U are the confluent hypergeometric functions for the case when $\gamma = 1$, relative rest, that respectively represents fermion and boson wave function.

$$\begin{aligned} \mathbf{u}^{\mathrm{f}}(r,n) &= \mathrm{e}^{-\kappa r}{}_1F_1 \left[\frac{n-1}{1+i}, n-1, (1+i)\kappa r \right], \\ \mathbf{u}^{\mathrm{b}}(r,n) &= \mathrm{e}^{-\kappa r} U \left[\frac{n-1}{1+i}, n-1, (1+i)\kappa r \right]. \end{aligned} \tag{2}$$

To construct the proton's strong force structure a product of the lower dimension solutions will be used and their scale ratios determine the mass, $m \sim= (\kappa_1 + \kappa_2 + \kappa_3)\hbar/c$. Similar to Eq. (1) there is a differential equation for the massless fields, Eq. (4), in the self-reference frame and it will be used to extract the lower dimension boson solutions [2], Table 3.

Total charge of a fermion particle is a mass independent quantity [30]. The three dimensional solution, $\mathbf{u}^{\mathrm{f}}(r,3)$, was used to represent the electron with the product field $\mathbf{u}^*(r)\mathbf{u}(r)$ representing the electrostatic **E** field [1]. In this derivation charge is quantized based on dimensions. For the case of the nuclear strong force the product $\Phi^*_{\text{strong force field}}\Phi_{\text{strong force field}}$ will be used to represent the strong force fields for the proton and neutron in a product of their component quarks.

$$\Phi_{\text{strong force field}} = \mathbf{u}^{\text{f}}(r,1) \cdot \mathbf{u}^{\text{f}}(r, 1D \text{ or } 2D) \cdot \mathbf{u}^{\text{f}}(r,2D). \tag{3}$$

The strong force field is treated as a simple static field, with no color boson, gluon, or exchange binding the components. The individual components are considered bound because only as a whole do they define their existence in the three dimensional laboratory frame, referenced to a common origin. No momentum distribution function for the quarks is considered that treat them as individual dynamic elements. The experimental justification for this is that the proton has no permanent or induced electric dipole moment, even though the component quarks possess spin and charge.

5. The Two-field Problem

Unlike the electron, the proton has two major fields: strong force and electrostatic. By analogy to the electron the massive fermion field made of three quark components support the strong force. We know the electrostatic field of the proton is very different from the electrons as on the mass scale the charge distribution of the proton is significantly larger because of its relative larger magnetic moment. The proton also has the boson characteristic of a weak charge. The proton's weak charge Q_{weak} exists and has been measured in spin-dependent electron scattering experiments off protons [41]. That implies that the proton is not only made up of fractional fermion components to generate the strong force, but also massive boson components to generate the electrostatic field and charge. The proton's lower mass relative to the neutron also implies the energy in the proton's electrostatic field may be proportionally lower as compared to the electrons which is $\sim 0.1\%$ of the total self energy [2]. This indicates a less compact charge density for the proton. Finally, the ability of deuterium to fuse under relatively modest conditions implies that the charge radius of the proton is indeed large.

Table 3. Spatial solutions, $u^{\text{family}}(r, \text{dimension})$, to the particle and field equations of the self-reference frame that generates the boson and fermion families for both massless fields and particles with mass [2,30]. The massive components are in boldface and the massless fields are not in boldface.

Dim.	Boson	Fermion	Note
No mass	Field	Field	
1	$u^{\text{b}}(r,1)$	$u^{\text{f}}(r,1)$	Bound
	Field formation	Neutrino formation	
2	$u^{\text{b}}(r,2)$	$u^{\text{f}}(r,2)$	Bound
3	$u^{\text{b}}(r,3) \rightarrow$ Photon	$u^{\text{f}}(r,3) \rightarrow \nu_e$	Free
Mass	Particle	Particle	
1	$\mathbf{u}^{\text{b}}(r,1)$	$\mathbf{u}^{\text{f}}(r,1) \rightarrow$ Down quark	Bound
	Charge formation		
2	$\mathbf{u}^{\text{b}}(r,2)$	$\mathbf{u}^{\text{f}}(r,2) \rightarrow$ Up quark	Bound
3	$\mathbf{u}^{\text{b}}(r,3) \rightarrow W^{\pm}\ Z^{o}$	$\mathbf{u}^{\text{f}}(r,3) \rightarrow$ Electron	Free

The massless form of the state function derived in equation 4 in the self-reference frame generates solutions dependent on dimension [30]. The 3D solution for the boson represents the photon, whereas, the 3D fermion solution represents the electron neutrino. The lower dimensional massless boson solutions will be used to assemble the long range field and the massive lower dimensional boson solutions will be used to generate the charge. These composite particles are more complex than the three dimensional case because they may require two static fields.

$$\frac{\partial^2 u(r)}{\partial r^2} + \left(\frac{n-1}{r}\right)\frac{\partial u(r)}{\partial r} + \kappa^2 \gamma u(r) = 0. \tag{4}$$

The massless field solutions respectively for the fermion and boson are:

$$\begin{aligned} u^{\mathrm{f}}(r,n) &= \mathrm{e}^{-i\kappa r}{}_1F_1\left[\frac{n-1}{2}, n-1, 2i\kappa r\right], \\ u^{\mathrm{b}}(r,n) &= \mathrm{e}^{-i\kappa r}U\left[\frac{n-1}{2}, n-1, 2i\kappa r\right]. \end{aligned} \tag{5}$$

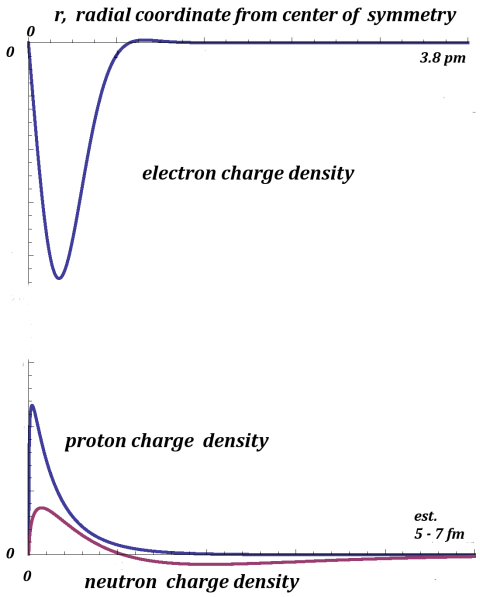

Figure 3. Computed electron, proton and neutron charge densities from self-reference frame state product functions. The neutron total charge is always zero independent of the quark component scales, whereas the proton charge is only totally positive when the up quarks have a scale difference of 2 or greater. Note the two radial scales are in pico meters for the electron and femto meters for the nucleons, their relative heights are set only for visual separation.

5.1. Generating charge density

The electron being a 3-D elementary particle its charge density is generated from, Gauss's law, the gradient of the electric field that is proportional to $\mathbf{E}(r) \sim u^*(r, n = 3)u(r, n = 3)$. This charge density when used to correct the hydrogen's atom Schrödinger equation solution using a singular potential, $1/r$, produces the bulk of the correction of the 1S state $\sim 99\%$ without a need for quantum electrodynamics [1]. This gives us some confidence that these structural solutions for particle composition are correct, Fig. 2.

The proton is a much more complex object with both a strong force field and electrostatic field. The fermion fractional quark solutions appear to generate the compact strong force potential. However, to generate the long range electrostatic field and its supporting charge the two sets of fractional boson components are required. The massive fractional boson components to generate the charge and the massless fractional components to generate the $1/r^2$ electric field. Support for this comes from the zero charge generated for the quark combination for the neutron. The neutron charge is always zero and independent of the quark scale ratio. We tested this numerically for a range of quarks scale ratios. This implies the neutron is very different in its ability to interact via the strong force because of this flexibility that is limited for the proton and its scale.

6. Strong Force Binding

The observable pieces of stable elementary matter, $n = 3$, are the electron, photon, electron neutrino. The massive boson $W^{\pm}$, Z^0 though not stable are solutions of equation 1 that have the charge and parity characteristics verified by experiment [30]. The composite structures: nucleons and mesons forms require more complexity to understand their assembly.

There are tests for the particle that can be made. The first test is for parity problems as a function of relative energy. The field elements should behave like a field and not like a particle, while also being stable. As individual fractional elements the lower dimensional components are not complete. However, in combinations of twos and threes they take on characteristics of three dimensional particles and fields that are actually found: mesons and baryons.

A self-reference frame description was given to the proton and neutron using products of one and two dimensional component solutions representing quarks [30]. What motivated these simple product representations for the composite particles is that for the proton there is no measurable electric dipole moment and the strong force is not plagued by parity violation, which these product forms satisfy using a common origin. With no electric dipole moment the ensemble of quarks would share the same center of symmetry. This makes a case for a potential interaction producing the strong force between nucleons as a contact interaction of overlapping density functions. In Table 3 there are no remaining freely propagating boson fields to represent the gluon. A nuclear strong force potential can be constructed from the products of the lower dimensional massive fermion components. The product of the solutions and its complex conjugate produces a density function that can be integrated to give a potential for the strong force. This is similar to how the electrostatic potential of the electron is generated [1]. The difference is the strong force potential is short range because the particle structures are compact, Table 4 and Fig. 4.

$$\mathbf{u}_{\text{proton}}(r) = \mathbf{u}^{\text{f}}(r, 1) \circ \mathbf{u}^{\text{f}}(r, 2) \circ \mathbf{u}^{\text{f}}(r, 2),$$

$$\mathbf{u}_{\text{neutron}}(r) = \mathbf{u}^{\text{f}}(r, 1) \circ \mathbf{u}^{\text{f}}(r, 1) \circ \mathbf{u}^{\text{f}}(r, 2), \tag{6}$$

$$\mathbf{u}_{6-\text{quarks}}(r) = \mathbf{u}^{\text{f}}(r, 1) \circ \mathbf{u}^{\text{f}}(r, 2) \circ \mathbf{u}^{\text{f}}(r, 2) \circ \mathbf{u}^{\text{f}}(r, 1) \circ \mathbf{u}^{\text{f}}(r, 1) \circ \mathbf{u}^{\text{f}}(r, 2).$$

Table 4. Nuclear characteristics.

Property	Cause
Bound independent nucleons	Compact potential
Zero proton dipole moment	Quark dynamics barred No parton distribution function
Nuclear mass defect	Quark Scale adjustment
Short range correlation	Six-quark state
Aggregate binding $A > 2$	Neutron-proton pair's Extend structure

7. Lab Frame Nucleon Structure

The compact strong force structure of the proton is generated from the relation in Eq. (6) allows a potential to be computed. This would be the strong force potential and not the electrostatic potential because it will be very short range. The potential can be computed outside of the core from the following integral.

$$V_{\text{strong}}(r) = \int_{\infty}^{r} \mathbf{u}^{*}_{\text{nucleon}}(x)\mathbf{u}_{\text{nucleon}}(x)\,\mathrm{d}x. \tag{7}$$

When the spin states are considered it is the proton–neutron pairs that allow for stable structures to be assembled.

7.1. Making deuterium

$$\frac{\hbar^2}{2m}\nabla^2\Phi - \frac{\hbar^2}{2mc^2}\frac{\partial^2\Phi}{\partial t^2} + i\hbar\frac{\partial\Phi}{\partial t} = V\left\{1 + \frac{V}{2mc^2}\right\}\Phi. \tag{8}$$

The full relativistic wave equation in the laboratory frame differs in two ways from the Schrödinger equation by having two additional terms [2]. The second order term in time and the quadratic term in the potential that is always repulsive. These are dropped for low energy bound state calculations assuming they are small. For binding the proton and neutron these two terms will not be used in a first approximation to solving the problem, Fig. 4.

Equation (7) computes the nuclear potential that is a simple exponential.

$$V_{\text{strong}}(R) = -V_{\text{o}}\mathrm{e}^{-\frac{2R}{\epsilon}} = -V_{\text{o}}\mathrm{e}^{-\alpha R}. \tag{9}$$

The nucleons' bound state differs a great deal from an atomic model. The reason being is that the nuclear potential is short ranged.

$$-\frac{\hbar^2}{2m}\nabla^2\Phi - V_o e^{-\alpha R}\Phi = E\Phi. \tag{10}$$

Equation (10) is solved in three dimensions for $\Phi(R,\theta,\phi,t) = U(R,\theta,\phi)G(t)$ much like the atomic central force problem. The method is laid out in [26] where first the angular variables are separated from the radial variable with

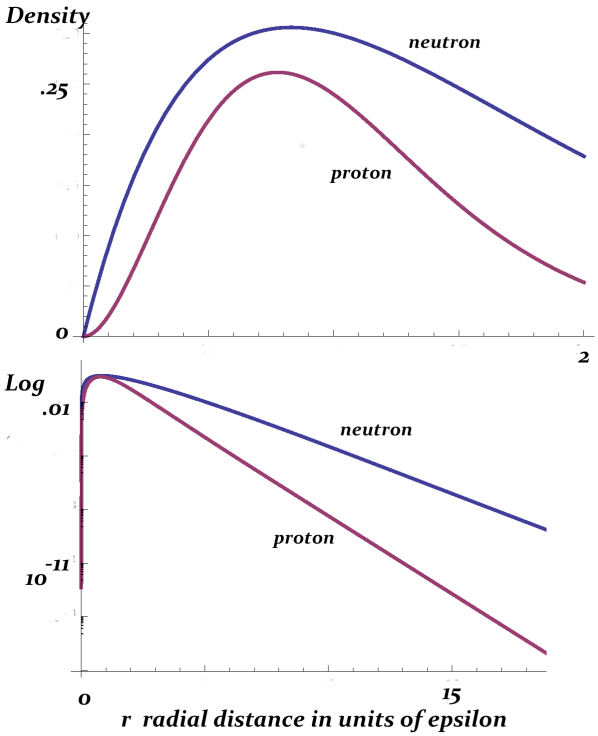

Figure 4. Computed proton and neutron density functions. Where density for the proton $\rho_{\text{proton}} = \mathbf{u}^{*\text{f}}(r,1)\mathbf{u}^{\text{f}}(r,1)\mathbf{u}^{*\text{f}}(r,2)\mathbf{u}^{\text{f}}(r,2)\mathbf{u}^{*\text{f}}(r,2)$ $\mathbf{u}^{\text{f}}(r,2)\ r^2$ from the three quark components and for the neutron $\rho_{\text{neutron}} = \mathbf{u}^{*f}(r,1)\mathbf{u}^{\text{f}}(r,1)\mathbf{u}^{*f}(r,1)\mathbf{u}^{\text{f}}(r,1)\mathbf{u}^{*f}(r,2)\mathbf{u}^{\text{f}}(r,2)\ r$.

separation constant, $l(l+1)$, that turns out to be in terms of the angular moment, l. The solutions with orbital angular momentum are defined in terms of the spherical harmonic functions, which in the nuclear strong force problem can be used to generate the nuclear quadrupole moment. Another force active in deuterium is the interaction of magnetic moments between the proton and neutron. Deuterium binding problem would not be complete unless details of the quadrupole moment were included. Traditionally the quadrupole momentum in deuterium is explained by the mixing of an *S* state and a *D* state in the bound potential [42]. Here the $l = 2$ angular solution mixed with the $l = 0$ principal solution generates the quadrapole moment for those nuclei with non-zero total spin

It is the radial solution, $l = 0$, that is of most interest $U(R,\theta,\phi) \longrightarrow \Phi(R)$ for the ground state. After separating variables an expression for three potential terms are missing: the electrostatic, the magnetic spin–spin interaction and spin–orbit interaction. For deuterium only one of these terms is important and that is the spin–spin interaction.

$$-\frac{\hbar^2}{2m}\left(\frac{\partial^2\Phi}{\partial R^2}+\frac{2}{R}\frac{\partial\Phi}{\partial R}\right)+\frac{l(l+1)}{R^2}\Phi - V_{\text{o}}\,\text{e}^{-\alpha R}\Phi = E\Phi. \tag{11}$$

This analysis starts by assuming the strong force potential term is dominant between a proton and neutron because of the overlapping unpaired *u* and *d* quarks. This is not a bad assumption because the orbital angular momentum in most

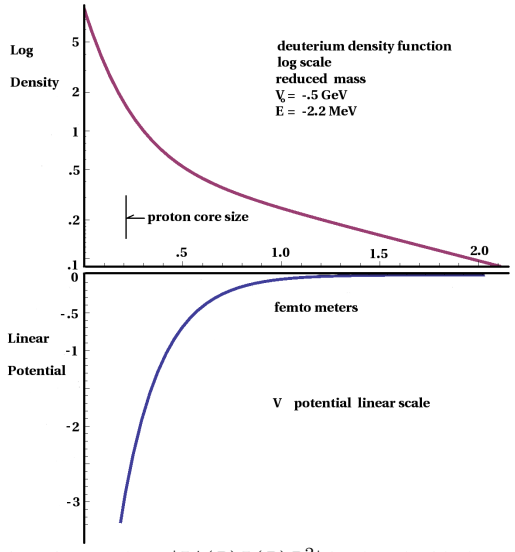

Figure 5. Density function of bound deuterium nucleus, $|\Phi^*(R)\Phi(R)R^2|$ is plotted with the potential. Figure from *yes Virginia, quantum mechanics can be understood* [2].

stable nuclei is zero. This forces a spherical symmetry on the bound state solutions with a central force while ignoring the spin–spin interaction (Fig. 5).

The solutions produced are in terms of the Bessel function $I_\nu(z)$ and $K_\nu(z)$. Only $I_\nu(z)$ solution represents a bound state as $K_\nu(z)$ continues to grow with *R*.

$$\Phi(R) = A\,\frac{1}{\alpha R}2^{\frac{1}{2}-i\frac{\sqrt{2mE}}{\hbar\alpha}}\left(\mathrm{e}^{-\alpha R}\right)^{-i\frac{\sqrt{2mE}}{\hbar\alpha}} \times\left(-\frac{2mV_\mathrm{o}\mathrm{e}^{-\alpha R}}{\hbar^2\alpha^2}\right)^{-i\frac{\sqrt{2mE}}{\hbar\alpha}} I_{-2i\frac{\sqrt{2mE}}{\hbar\alpha}}\left(2\frac{\sqrt{2mV_\mathrm{o}\mathrm{e}^{-\alpha R}}}{\hbar\alpha}\right). \tag{12}$$

The nuclear binding of deuterium is determined by the nucleon mass defect driven by the core overlap of the two nucleons. Whereas, for the bulk of the volume the nucleons behave as single well defined particles. This is expected because the narrow nuclear potential will force the wave function to extend away from the center of symmetry in a second slower decaying exponential. The scale of the bound state is large relative to the individual nucleon core radii. This structural feature may aid deuterium fusion at a close approach.

Setting $\beta = \sqrt{E/2mc^2}$, where β is small >10^{-4} then the density function reduces to

$$\Phi^*(R)\Phi(R)R^2 = \frac{A^*A}{2}\epsilon^2 I_{2i\beta}\left(2\mathrm{e}^{-\frac{R}{\epsilon}}\sqrt{\frac{V_\mathrm{o}}{2mc^2}}\right)\times I_{-2i\beta}\left(2\,\mathrm{e}^{-\frac{R}{\epsilon}}\sqrt{\frac{V_\mathrm{o}}{2mc^2}}\right). \tag{13}$$

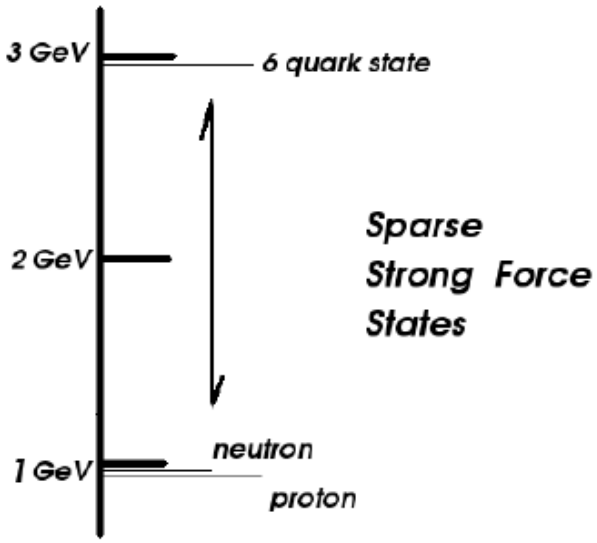

Figure 6. Combined six-quark state showing the sparse distribution of prompt baryon states.

8. High Energy Proton–Neutron State

From electron–nucleon scattering experiments to detect nuclear short range correlation both the internal momentum of nuclear components and the threshold for strong proton-neutron short range correlations can be extracted [40]. This momentum data matches the modeling of deuterium in the previous section for the strong force calculation showing a double exponential decay in both the real and momentum space density functions [30]. These experiments also eliminate any possibility of there being deep state electrons in the structure as they would be easily detected in the scattering experiments.

Using statistically independent spaces for particles and fields forced the abandonment of the point particle descriptions and replaces it with a structured particle properties. This allows including the nucleon's component quarks to form high energy compact particles totally unlike the low energy elementary three dimensional lepton, electron. Particle structure overlap for nucleons can be computed to generate the strong force's static potential function. Models using an exchange of boson analogous to photon emission and absorption do not appear to be required for either binding or in modeling scattering experiments.

The use of this simple model in the case of deuterium has proven useful in both being able to define binding of the two nucleons [2] and defining the high energy state when the proton is driven into the neutron to form the short range correlated structure. This latter condition computed from the excess energy, 1 GeV, required to form a six quark state shown in Fig. 6. This energy is taken from the reduced scale of the six-quark state. The excess energy required for the high energy state comes from the reduced scale the entire structure and is the simplest behavior that occurs promptly on collision. The six-quark state will not form until an extra 1 GeV of energy can be externally supplied either by an accelerator driven collision or in a massive astrophysical object, a neutron star near its upper mass limit (Fig. 7).

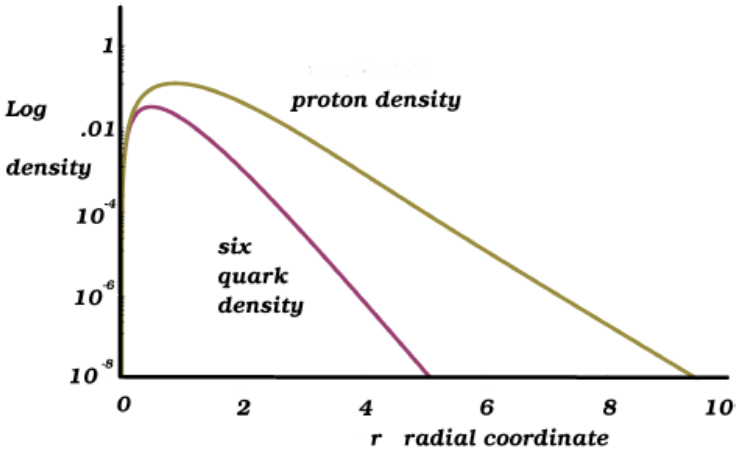

Figure 7. Scale reduction to the six-quark state is a factor three, not two and that requires an extra 1GeV over the rest energy of the two nucleons to be accomplished.

8.1. Nuclear short range correlation for heavier isotopes

Schematically the momentum space data from the short-range correlation experiments can be represented in a simple graph that has three parts [40]. The first part is the dominate low momentum peak in the deuterium data where the nucleons spend some of their time with low momentum with no third particle constraints limiting their motion. As

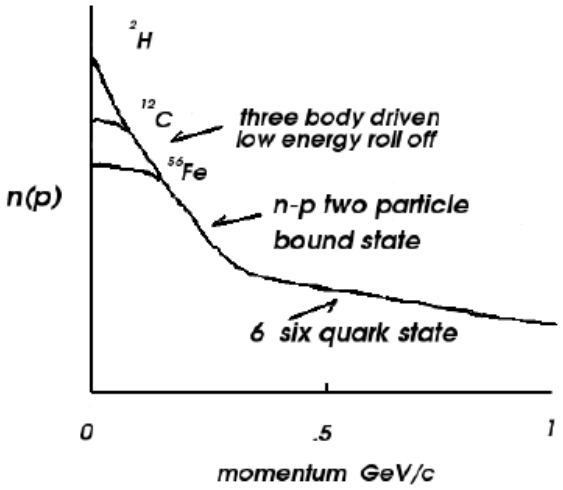

Figure 8. Measured log momentum density from high energy electron scattering not only shows the n–p correlation for deuterium, but the confinement effect of the three body interaction at high nucleon counts in the roll off of the zero momentum peak [40].

nucleons are added the low momentum behavior around $p = 0$ is suppressed as other two body interaction occur. The unchanging intermediate momentum for increasing nuclei count suggestion this behavior is universal as isotope mass is increased squeezing down region in the middle section in Fig. 8. The third high momentum region remains a fixed feature is the short-range correlation in the high energy tail. Over this wide energy range the spectroscopy is not very rich, meaning there are few available states other than the two particle interactions and the six-quark state. This is very different when compared to solid state models with a high density of states that are commonly misused to model nuclear matter.

8.2. Implications for binding $A > 2$

The implication from more recent accelerator experiments [43] probing the nucleus with electrons allows nuclear binding to be reduced to a structure dependent property, without considering deep states that do not exist or meson binding intermediaries. By finding the first prompt state of deuterium at $\sim$1 GeV above the self-energy of deuterium when the proton and neutron are forced to be one removes a great deal of confusion. Then electron probing below this threshold for short range correlation, which translates to less than $\sim$4.5 GeV for the electron input energy permits the internal momentum distribution of the proton in deuterium and heavier nucleons to be more accurately probed. This yields a picture of the deuterium density function than can be consumed in binding with additional nucleons.

The deuterium nucleus in Fig. 5 shows two distinct regions: a well defined core and a wider regions extending outwards. It is the broader structure that represents the low momentum values of the nucleons that can interact and attract other nucleons. Though this portion of the density function only represents 10% of the particle's density, its reach allows other nucleons and other proton-neutron pairs to bind. Evidence can be seen in data of recent accelerator experiment measuring the momentum distribution for knocked out protons from deuterium, tritium, and ^{3}He, as the exterior portion of the deuterium wave function is consumed in the binding of the additional nucleon [43]. This data is recorded as the ratio in cross section of protons knocked out from tritium and ^{3}He scale to deuterium at the minimum measured internal proton momentum. This measured ratio is well less than 1 in tritium and ^{3}He indicating the low momentum or spatially extended part of the wave function of deuterium has been truncated and now forms a bond with greater particle momentum. This was also evident in the early short range correlation measurements for heavier nucleons as shown in Fig. 8. The conclusion is that the proton–neutron pair constitutes the basis to build heavier nucleons because of their extended structure and facilitates fusion.

9. D–D Fusion

Standard D–D fusion proceeds on two equally probable paths if there is sufficient energy to drive the ions together in free space.

$$\begin{aligned} {}^2\mathrm{H} + {}^2\mathrm{H} &\rightarrow {}^3\mathrm{H} + \mathrm{n} + 17.6\ \mathrm{MeV}\ \ 50\%, \\ {}^2\mathrm{H} + {}^2\mathrm{H} &\rightarrow {}^3\mathrm{He} + \mathrm{p} + 4.03\ \mathrm{MeV}\ \ 50\%. \end{aligned} \tag{14}$$

One feature of D–D fusion reaction found in D–D scattering cross section data is that no abrupt lower bound cut off for fusion as a function of colliding particle energy is found. The important feature allowing fusion is that both energy and momentum are conserved requiring multiple final state products. The process in question, Eq. (15) does not have this pathway to conserve both energy and momentum unless there is some other element to carry off the energy. Gamma emission is suppressed in low energy encounters. That only leaves an external particle participating to carry off the energy and momentum.

$$^2\mathrm{H} + {}^2\mathrm{H} \rightarrow {}^4\mathrm{He}^* + \sum_i \Delta E(e_i) \rightarrow {}^4\mathrm{He} + \text{heat}. \tag{15}$$

For free particle interaction this third process is not observed as there is nothing to remove the 24 MeV excess energy. The first two reaction are not dominant in the solid state as the quantities of tritium and helium-3 are only found in trace amounts, whereas, there are significant correlated findings of both helium-4 and heat.

9.1. Loss mechanism

During nuclear fusion when a proton and neutron combine, the masses of the components are reduced and the excess energy will be shed. The electrostatic field of the proton and neutron will be altered in the region of the core even though its charge remains constant. The change in the charge distribution and associated energy change is absorbed in the mass change allowing energy to be shed directly to lattice electrons coupled to the change in baryon charge density distribution through the electrostatic field. This can be represented as a time dependent interaction potential, $V_{\text{int}}(t)$.

$$V_{\text{int}}(t) \sim \iint \frac{\rho_{\text{electron}}(r)\rho_{\text{baryon}}(r',t)}{\mid \mathbf{r} - \mathbf{r}' \mid} r'^2 r^2 \mathrm{d}r' \; \mathrm{d}r. \tag{16}$$

If the mass defect energy from fusion can be acquired by electron currents local to the nucleus then the normal fusion processes will be short circuited and the energy will be deposited into the valence electrons. Nickel and Palladium possess a band structure, a characteristic not shared by any other metals to allow this process.

9.1.1. *Nuclear polarization*

The scale of the electron charge sets the minimum range where dynamic screening is effectively provided by the valence electron and this is on the order of 4×10^{-13} m. To further close this range the non-linear response of the lattice so that the nuclear attraction can overcome the electrostatic repulsion. It is only possible to estimate the cross over point once the charge structure of the nucleus is known as well as the strong force polarization.

The incremental energy transfer to valence electron current is not a quantized process because the energy states of the nucleus are dependent on the scale relationship between the nucleon quarks, which appear to vary continuously. The low levels of residual radiation from tritium production indicates that the incremental loss of energy to the lattice is the most active component and it rarely produces a single high energy transition to a lattice electron carrying MeV energy. The flexibility that is obtained in the incremental energy loss is due to the three-body behavior of the quark's scale in adjusting nucleon mass. The neutron is the most compliant in terms of energy verses its quark scaling. This compliance lets the internal quark scale adjustments bind nucleons in the fusion process [2]. Compliance means that the up-down quark scale ratio can vary more for a smaller change in nucleon rest energy in the neutron verses the proton.

Interrupting the loss process requires the question to be asked: Is the energy transference reversible? The answer to this is that it is improbable because it would require extraction of energy from the valence electrons at the prevailing temperature. The local heat capacity in the electron gas is insignificant when compared with the energies involved in the nuclear process. This makes the reversal of the process highly unlikely in terrestrial environments.

The scale over which this process occurs is fixed by the details of the approach of the two nucleons to minimize the electrostatic potential and maximize the strong force attraction. EM and weak force polarization is understood and that has to be extended to the strong force. In the schematic of the approach of two deuterium ions shown in Eq. (17), the lower figure would represent a favorable polarization for fusion.

Table 5. Guide to the sequence of events that lead to fusion in the FCC lattice and the dumping of heat into the lattice by a direct potential interaction between the fusing deuterium ions and dynamics screening currents that are supported in some FCC metals. The number of steps in this process are reflected in the difficulty of engineering a large scale process. Column three represents the mechanically alloyed Ni–Pd interface and the diffusion Ni–Cu boundary.

▼	⟸ Damage Controlled	
	Mechanical alloying controlled ⟹	▼
1	Absorption of deuterium into Pd, Ni, or Ti	1
2	Strong near surface $> 1\mu$m damage gradient	
3	Hydride formation, bulk lattice expansion, stacking fault generation (Ti)	
4	Vacancy formation and coalescence into microvoids	
5	Damage and hydride forced expansion of the untransformed volume	
6	Deuterium wetting of interior of microvoids	
7	Microvoid collapse into prismatic dislocation loop	
8	Microvoid collapse ejecting ^{2}H ions into local matrix	
	Mechanically alloy Ni–Pd interface	2
	Ni–Cu diffusion boundary	
9	Dual ^{2}H ions split on a $\langle 111 \rangle$ axis centered symmetric FCC octahedral site	3
10	Symmetric closed die forge, compression enhanced by anharmonic lattice vibrations	4
11	Dynamic screening of dual ^{2}H ions by valence electron 6-axis current flow	5
12	Overlap of neutron and proton wave function releases energy to screening currents	5
13	Adjustment of nucleon charge distribution via potential interaction to screening currents	7
14	Irreversible energy shedding to the current as proton charge distribution adjusts	8
15	Final energy transfer via a potential interaction interaction with screening electrons	9
16	Lattice supported D–D fusion	10

$$\begin{aligned} \{\mathbf{N}-\mathbf{P}\} \dashrightarrow \quad \dashleftarrow \{\mathbf{N}-\mathbf{P}\}, \\ \{\mathbf{P}-\mathbf{N}\} \dashrightarrow \quad \dashleftarrow \{\mathbf{N}-\mathbf{P}\}. \end{aligned} \tag{17}$$

The question is what kind of attractive force is generated between two neutrons already in a bound structure?

This is expected to be very different than what is found between two free neutrons. A reflection of this can be found in the old accelerator measurements that searched for a threshold in D–D fusion, none was found, only a roll off in cross section as interaction energies fell below 10 keV. At these low energies the force amplification on the interstitial site from anharmonic [21] localization of lattice vibration can drive the fusion process to completion assisted by the increasing nuclear attraction as the excess energy is removed by electronic currents (Table 5).

10. Discussion

The importance of the experimental cold fusion work started by Fleischmann and Pons [8] opened a window on the workings of the nucleus where a unique low energy view is supplied. Before a serious examination of the nucleus and cold fusion could take place the problems with quantum mechanics had to be resolved: structure of the participating components and polarization [44]. It was known since the early 1930s that quantum mechanics was in need of a serious overhaul [27,45–48]. The strong force is the most complex of the forces and the most difficult to handle. The barrier to modeling cold fusion was a poor understanding of the strong force, because of the binding mechanism the standard model tried to impose. Specifically, the requirement for a fictitious complex field called the gluon. Once the gluon was discarded it was possible to look at the lattice fusion process in detail after the metallurgical preliminaries were clarified. For the more general problems of particle physics the mechanisms used for assembling the baryons and their respective charges out of fractional fermion and boson components opens a path for building the other family of particles.

The minimal D–D fusion process in metals requires a complex chain of events (Table 5) with a favorable crystal and band structure making the process difficult to trigger. The recent accelerator experimental evidence of external electrons directly participating in the nuclear fusion process [33] added the lattice electron as a candidate to mediated nuclear fusion to the standard processes of transmutation: alpha, beta, electron capture, fission, and gamma emission. The solid state fusion process of two deuterium ions occupying a single FCC octahedral interstitial site presents some experimental challenges, because the residence time is probably a picosecond or less. A signal to the process was found in the spectrum of electromagnetic radiation that is normally a very weak emission that appears to be pumped by intense screening currents in M. Swartz active MASER at 327 MHz. The triplet to single transition from lattice bound atomic deuterium being strongly pumped by local currents in an active cold fusion specimen Pd–D embedded in ZrO_2 provides some proof of the role of electronic currents in the loss mechanisms driven by lattice fusion.

Acknowledgments

The most important source of information for this paper were the many failed attempts to generate physical results as this large body of work narrowed the range of possible mechanisms.

References

[1] J. Wallace and M. Wallace, Electrostatics, in: G. Meyneni(Ed.), *Science and Technology of Ingot Niobium for Superconducting Radio Frequency Applications*, AIP Conf. Proc., Vol. 1687 (AIP Melville, NY 2015) 040004-1-14.

[2] J. Wallace and M. Wallace, *yes Virginia, Quantum Mechanics can be Understood*, Casting Analysis Corp., Weyers Cave, VA, 2017.

[3] A. Carpinteri, G. Lacidogna and A. Manuello (Eds.), *Acoustic, Electromagnetic, Neutron Emission from Fracture and Earthquakes*, Spriner, Switzerland, 2015.

[4] G. Egely, Transmutation by dust fusion, *Infinite Energy* **130** (2016) 19–25.

[5] L. Jaitner, *The Theory of Condensed Plasmoids and Low Energy Nuclear Reactions*, preprint, www.condensed-plasmoids.com 2015–2019.

[6] Borexino Collaboration, Comprehensive Measurement of pp-chain solar neutrino, *Nature* **562** (2018) 505–510.
[7] J.P. Wallace and M.J. Wallace, *Refraction*, 2018, http://viXra.org/pdf/1809.0582v2.pdf.
[8] M. Fleischmann, S. Pons and M. Hawkins, *J. Electroanal. Chem*. **261** (2A) (1989) 301.
[9] Y. Iwamura, S. Murakami and J. Kasagi, Excess energy genertion using a nano-sized multilayer metal composite and hydrogen gas, *J. Condensed Matter Nucl. Sci.*, submitted.
[10] T. Mizuno and J. Rothwell, Increased excess heat from palladium deposited on nickel, preprint, https://www.lenr-canr.org/acrobat/MizunoTexcessheat.pdf.
[11] F. Celani, C. Lorenzetti, G. Vassallo, E. Purchi, S. Fiorilla, S. Cupellini, M. Nakamura, P. Boccanera, R. Burri and A. Sapllone, First evaluation of coated constantan wires comprising Capuchin knots to increase anomalous heat and reduce input power at high temperature, *J. Condensed Matter Nucl. Sci.* **29** (2019) 52–74.
[12] Y. Fukai and W. Okuma, Formation of superabundant vacancies in Pd hydride under high pressures, *Phys. Rev. Lett.* **73** (1994) 1640–1643.
[13] E. Storm, Anomalous energy produced by PdD, *J. Condensed Matter Nucl. Phys.* **20** (2016) 81–99.
[14] K. Sakai, M. Mizuno, H. Araki and Y. Shirai, The effect of the hydrogenation process on the production of lattice defects in Pd, *J. Alloys Compounds* **414** (2006) 204–206.
[15] J. Wallace, *Positron Interactions with Vacancies and Dislocations*, D. Eng. Sc., thesis, Columbia Univ. NY, 1975.
[16] R. Golpaliengar, J. Wallace and R. Oriani, *Mat. Sci. Eng*. **85** (1984) 191.
[17] M. Swartz, Atomic deuterium in active LANR systems produce 327.37 MHz Superhyperfine RF MASER emission, ICCF-22 Abstract, Sept. 2019.
[18] J. Li, R. Oriani and L. Darken, The thermodynamics of stressed solids, *Zeit. Phys. Chem.* **49** (1966) 271–290.
[19] M. Swartz, *J. Condensed Matter Nucl. Sci.* **15** (2015) 102–105.
[20] M. Swartz, G. Verner, J. Tolleson, L. Wright, R. Goldbaum and P. Hagelstein, *J. Condensed Matter Nucl. Sci.* **15** (2013) 66–80.
[21] V.I. Dubinko and D.V. Laptev, Chemical and nuclear catalysis driven by anharmonic vibrations, *Lets. Materials* **6**(1) 16–21.
[22] J. Wallace, Proton in SRF niobium, in G. Myneni (Ed.), *SSTIN10 AIP Conference Proc. 1352*, AIP, Melville, NY, 2011.
[23] J. Wallace, G. Myneni and R. Pike, Curvature, Hydrogen, and Q, in: G. Myneni(Ed.), *SSTIN10 AIP Conf. Proc. 1352*, AIP, Melville, NY, 2011, pp. 33–46.
[24] J.P. Biberian, Transmutations, *J. Condensed Matter Nucl. Sci.*, 2019, to be published.
[25] R.W. Cahn, Recovery and recrystallization, in: R.W. Cahn(Ed.), *Physical Metallurgy*, North-Holland, Amsterdam, 1970, pp. 1129–1198.
[26] H. Bethe and E. Salpeter, *Quantum Mechanics of One- and Two-Electron Atoms*, Springer, Berlin, 1957.
[27] P. Dirac, *Relativistic quantum mechanics*, *Proc. Royal Soc.* **A 136** (1932) 453.
[28] H. Foley and P. Kusch, *Phys. Rev.* **73** (1948) 412.
[29] W. Lamb, *Phys. Rev.* **72**(3) (1947) 241.
[30] J. Wallace and M. Wallace, *The Principles of Matter Amending Quantum Mechanics*, Casting Analysis Corp., Weyers Cave, VA, 2014.
[31] V. Moruzzi, J. Janak and A. Williams, *Calculated Electronic Properties of Metals*, Pergamon, NYC, 1978.
[32] P. Kalman and T. Keszthelyi, Solid state internal conversion, *Phys. Rev. C* **69** (2004) 031606(R).
[33] M. Liboglavsek, *J. Condensed Matter Nucl. Sci.* (2019) to be published.
[34] J. Dauben, *George Cantor His Mathematics and Collaboration*, Harvard Univ. Press, Cambridge, MA, 1979.
[35] G. Cantor, *J. für die reine und angewandte Mathematik* **84** (1887) 242.
[36] W. Heisenberg, *The Physical Principles of the Quantum Theory*, Univ. Chicago Press, Chicago, IL, 1930.
[37] J. von Neumann, *Mathematical Foundations of Quantum Mechanics*, Princeton Univ. Press, 1932, translation 1953.
[38] J. Friedman and H. Kendall, Deep inelastic scattering, *Ann. Rev. Nucl. Sci.* **22** (1972) 203–254.
[39] M. Gell-Mann, Symmetries of baryons and mesons, *Phys. Rev.* **125** (1962) 1067–1084.
[40] J. Arrington, D. Higinbotham, G. Rosner and M. Sargsian, Hard probes of short-range nucleon–nucleon correlations, 2012, arXiv:1104.1196v3 [nucl-ex].
[41] Q_{weak} Collaboration Jefferson Lab., *Nature* **557** (2018) 207.
[42] E. Fermi, *Nuclear Physics*, (Univ. Chicago Press, Chicago, IL 1949.

[43] Tritium Collaboration Jefferson Lab. Hall A, Comparing proton momentum distribution in $A = 2, 3$ nuclei via ^{2}H, ^{3}H, and ^{3}He (e,e'p) measurement, arXiv 1902.06358v3 [nucl-ex] (2019).
[44] J. P. Wallace and M.J. Wallace, Refraction, http://viXra.org/pdf/1809.0582v3.pdf, 2018.
[45] G. Gamow, *Thirty Years that Shook Physics*, Anchor Books, NY, 1966.
[46] A. Einstein, B. Pololsky and N. Rosen, *Phys. Rev*. **47** (1935) 777.
[47] Y. Aharonov and D. Bohm, *Phys. Rev*. **115** (1959) 485.
[48] J. Bell, On Einstein, Polodsky, and Rosen Paradox, *Physics* **1**(3) (1964) 195.
[49] J. Wallace, G. Myneni, M. Wallace, R. Pike and G. Westphal, *Terrestrial Nuclear Processes*, Casting Analysis Corp., Weyers Cave, VA, 2012.